



# The potential use of straw-derived biochar as the adsorbent for La(III) and Nd(III) removal in aqueous solutions

Qingzhou Zhao<sup>1,2</sup> · Yanfen Wang<sup>3</sup> · Zhihong Xu<sup>2</sup> · Zhisheng Yu<sup>1</sup>

Received: 17 July 2020 / Accepted: 13 April 2021 / Published online: 22 April 2021

© The Author(s), under exclusive licence to Springer-Verlag GmbH Germany, part of Springer Nature 2021

## Abstract

Recent attention on the lanthanides (Ln) contaminant such as lanthanum (La) and neodymium (Nd) extensively used in industry has aroused the great desire for the effective adsorbent. Biochar, relying on its high selectivity and optional ease, is regarded as a promising adsorbent for lanthanides removal although the evaluation of the efficiency and mechanism of La(III) and Nd(III) adsorption on biochar still lags. Here, we investigated the aqueous adsorption processes through SEM, TEM, EDS, FTIR and Raman spectra, XPS, and batch experiments. The porous structure of biochar and the complex functional groups on its surface contributed to the La(III) and Nd(III) removal processes. The kinetic of La(III) and Nd(III) adsorption agreed well with the pseudo-second-order kinetic model. The adsorption capacity showed a strong positive correlation with pH value. However, it was only slightly altered and robust in La(III) and Nd(III) adsorption respectively. The isotherm results reflected significant fitting to the Sips model as well as Langmuir and Freundlich model. Thermodynamic demonstrated the spontaneity, endothermic nature, and temperature favor of the adsorptions on biochar surface (La:  $\Delta H^0=35.39$  (kJ/Mol),  $\Delta S^0=104.71$ (J\*Mol<sup>-1</sup>\*K<sup>-1</sup>) and  $\Delta G^0<0$ ; Nd:  $\Delta H^0=16.71$ (KJ/mol),  $\Delta S^0=119.41$ (J\*Mol<sup>-1</sup>\*K<sup>-1</sup>) and  $\Delta G^0<0$ ). Both the La(III) and Nd(III) removal processes combined physical and chemical adsorptions. Therefore, biochar could be a potential green material for the lanthanum and neodymium adsorption with high efficiency.

**Keywords** Biochar · Adsorption mechanism · Lanthanum · Neodymium

## Introduction

With the enormous progress on rare earth elements (REE) in the past decades, lanthanides (Ln) were applied into the industry for the manufacture of optic filters, electronics components, hydrogen storage, artistic glasses, and steel modifiers (Parks et al. 2013; Tan et al. 2014). Unfortunately, via the industrial sewages carrying the REE, the rare earth waste raised severe environmental contamination and threatened

human health (Johnson et al. 2012; Kuta et al. 2011; Liao et al. 2018; Tan et al. 2014). Thus, the practicable and efficient methods for removal of neodymium (Nd) and lanthanum (La), which are the typical nuclides belongs to the first triad of the lanthanide series, were actively pursued (Galunin et al. 2010; Kusurini et al. 2018; Tan et al. 2014). To eliminate the environmental influence of the pursued (Galunin et al. 2010; Kusurini et al. 2018; Tan et al. 2014). To eliminate the environmental influence of the radioactive REE sewages, various techniques such as reverse osmosis, evaporation, solvent extraction, chemical precipitation, membrane separation ion-exchange, and adsorption were attempted to extract the contaminants in the wastewater before they were discharged into the environment (Kusurini et al. 2018; Meunier et al. 2006; Oehmen et al. 2006; Torab-Mostaedi et al. 2013). Adsorption gathered the most attention among these methods due to its low cost, high selectivity, and operational ease (Liao et al. 2018; Zhou et al. 2018). Because of the highly adsorptive properties of lanthanides, mineral particles, colloids and natural organic matter all could bind to the nuclides to limit their migration and diffusion into the environment (Johnson et al.

Responsible Editor: Philippe Garrigues

✉ Zhisheng Yu  
yuzs@ucas.ac.cn

<sup>1</sup> College of Resources and Environment, University of Chinese Academy of Science, 19 A Yuquan Road, Shijingshan District, Beijing 100049, People's Republic of China

<sup>2</sup> Environmental Futures Research Institute, Griffith University, QLD, Nathan 4111, Australia

<sup>3</sup> College of Life Science, University of Chinese Academy of Sciences, 19 A Yuquan Road, Beijing 100049, People's Republic of China

2012; Tan et al. 2014). Especially, mineral particles play the key role of pivotal sorbents to regulate the fate and transport of Nd and La in nature (Cremel et al. 2007; Kumar et al. 2012). Potent absorbents with high-affinity could remediate the environmental contamination and recover resources through the collection of lanthanides at trace and ultra-trace levels (Johnson et al. 2012; Sharma and Tomar 2011; Shi et al. 2012; Tan et al. 2014). Unfortunately, the adsorption capacity and efficiency of most existing absorbents still need to be improved further. Thus, a novel material as a more ideal candidate of absorbent to lanthanides removal was intensely desired.

Biochar, the pyrogenic carbonaceous residue prepared through thermal degradation, receives increasing attention for being the potential substitute of the ideal adsorbent to sewage contamination. Biochar is derived from the pyrolysis process of carbon-rich biomass with an oxygen-limited environment. A large range of feedstock materials makes biochar multifunctional so that it is widely used in environmental remediation (Inyang et al. 2015; Mohan et al. 2014). The biochar adsorption is implemented based on the mechanism electronically attracting the positive ion by its negative surface (Inyang et al. 2015). In addition, the biochar could also transform contaminants into composites and participates through surface interaction (Cao and Harris 2010; Dong et al. 2011; Wang et al. 2015). Compared to activated carbon, the most prevalent carbonaceous sorbent prepared by pyrolysis as well, biochar shares the primary production characteristics including surface heterogeneity, high microporosity, and superficial area with it (Ahmad et al. 2014; Cao et al. 2011). Nevertheless, biochar is generally directly applied for adsorption rather than modified by thermal or chemical activation to enhance the surface properties like activated carbon (Ahmad et al. 2012; Ahmad et al. 2014; Cao and Harris 2010). The diversification of the preparation condition in terms of feedstock source, retention time, and pyrolysis temperature generates the biochar with diverse physical, chemical, and mechanical characteristics. Thus, biochar acquires the flexibility to extend its applicability for adsorption to the environmental contaminants by being optimized into the most efficacious sorbent. Surprisingly, despite some studies on the aqueous lanthanide elimination by traditional sorbents, the application of biochar adsorption for the lanthanide removal remains unknown. Therefore, it is urgent to understand the effect and mechanism of the biochar adsorption to Neodymium (Nd) and Lanthanum (La) in an aqueous solution.

To clarify the mechanism of biochar adsorption for Nd(III) and La(III) removal, a batch experiment was performed in this study. Treatments with the various contact time, temperatures, and pH were conducted to investigate the adsorption kinetics, thermodynamic, and adsorption mechanism. The biochar

prepared by wheat straw was also characterized by XRD, SEM, TEM, XPS, and FT-IR respectively.

## Method and material

### Biochar preparation

The biochar was produced using straws of wheat (*Triticum aestivum*) as the feedstock. After the oven at 60 °C to dry the straws for 24h, biochar was prepared through pyrolysis in an oxygen-insulated environment with a temperature of 400 °C and the retention time of 2 h. All this process was carried in a custom-made stainless steel furnace. The collected biochar was sieved by 0.2 mm sieves for characterization and the experiment in batch mode.

### Biochar characterization

The scanning electron microscopy (SEM, 15 JSM-6360LV) was employed to acquire the morphological images on the biochar surface. Since the biochar possessed a large number of intra-pores, transmission electron microscopy (TEM, JEM-1011) was also performed to observe the porous structure of biochar. The biochar particles were scanned using Fourier transform infrared spectroscopy (FTIR, Thermo Nicolet, 8700, Madison, WI, USA) Raman spectra (Mettler Toledo, Zurich, Switzerland) in the range of 4000–400  $\text{cm}^{-1}$  and 2000–400  $\text{cm}^{-1}$  respectively to determine the functional groups on the surface. The dipole moment changes resulted from various vibrational modes of groups on biochar make their adsorption peak suitable to either FTIR or Raman spectra. The spectra quality of two vibrational spectroscopies also depends on the size and type of detectable particles. Thus, the combination of FTIR or Raman spectra could be a complement to imply the structural information of molecules on biochar (Chi et al. 2017; Kappler et al. 2016). With a monochromatized Al-K $\alpha$  X-ray ( $h\nu = 1486.6$  eV) serving as the radiation source, the element analysis was performed on the X-ray photoelectron spectroscopy (XPS, Thermo ESCALAB250 analyzer) accompanying 20eV pass energy constantly. The binding energies of the photoelectrons were also calibrated by the C1s peak at 284.8 eV. The O1s photoelectrons resulted in the peak at a binding energy of 532.7 eV.

### Batch experiment

The adsorption experiments were conducted in batch mode with the aqueous Neodymium and Lanthanum solution in the polyethylene centrifuge tubes. No attempts were applied to regulation the ambient condition of the treatments. The stock solution of Nd(III) and La(III) with various volumes were added for achieving the desired initial concentration.

Various doses of biochar were successively added to the aqueous solution. NaOH or HCl solution with a negligible volume of 0.01 and 0.1 mol/L were used for adjustment for the target pH in the system. The polyethylene centrifuge tubes were shaken with the end-over-end tumbler for the adsorption equilibrium. The centrifugation with 9000rpm for 40 min was employed to separate the liquid and solid phases. The determination of the Nd(III) and La(III) concentration was performed on the spectrophotometer. To avoid bringing the Nd(III) and La(III) loss on the centrifuge tube wall in the biochar adsorption process, curves of control treatment with or without biochar were both calibrated. The adsorbed mass of Nd(III) and La(III) was subsequently computed according to the deduction of the solution mass from the mass spike. All the collected data were based on the average of the repeated measurements for three duplications. Only the data with fractional errors limited in 5% were employed.

## Results and discussion

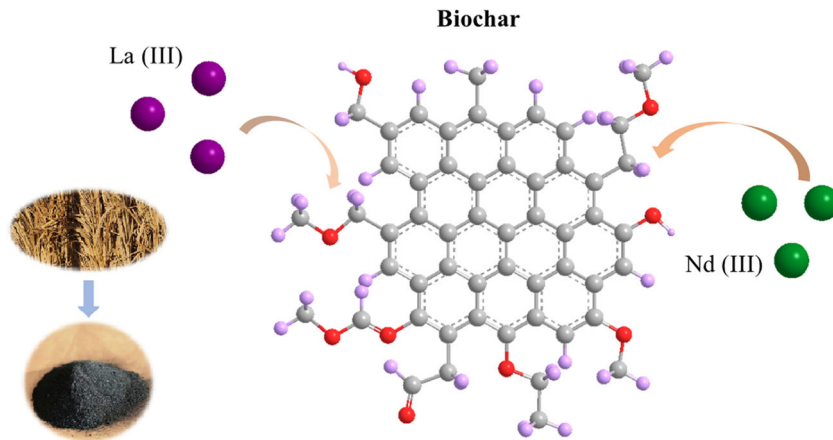
In this study, the adsorption processes for lanthanides such as La(III) and Nd(III) were performed taking biochar prepared from a wheat straw as the adsorbent. The derived biochar mainly consisted of irregular stacks with the deposition of stable aromatic rings (Chen et al. 2019; Lehmann et al. 2020) (Fig. 1). Numerous functional groups such as carbonyl, carboxyl, and hydroxyl groups formed on the biochar surface. These alkaline or oxygen-containing functional groups provided biochar competent adsorption capacity for La(III) and Nd(III) removal (Antón-Herrero et al. 2018; Chen et al. 2019).

## Characterization

### SEM, TEM, and EDS

Figure 2 depicted the porous structure of the biochar before and after the La(III) and Nd(III) uptake using SEM and TEM.

**Fig. 1** Biochar preparation and La (III) and Nd (III) adsorption mechanism on biochar



The raw biochar without the lanthanides removal presented smooth pore walls on the external and internal surfaces. After the adsorption, the biochar became coarse and bumpy on the surface. In fact, this roughness could be attributed to the corrosion on the biochar surface and coating of adsorbed lanthanides ions in either La(III) or Nd(III) removal (Liu et al. 2020). There was no peak observed from the EDS spectra results of the raw biochar. Nevertheless, peaks represented La(III) and Nd(III) occurred in the statistics of the biochar after respective adsorption processes (Fig. S1). These findings revealed the ion exchange and binding of the lanthanides contaminant on the sorbent surface, which were the main forms of the biochar sorption.

### FTIR and Raman spectrum analysis

To explore the functional groups on the biochar surface, FTIR spectra data were presented in Fig. 3A. The FTIR spectra of the raw, La(III) adsorbed and Nd(III) adsorbed biochar in the wave region of 400–4000  $\text{cm}^{-1}$  demonstrated the presence and participation of the functional groups such as C–C, C=O, C–H, and –OH in the sorption processes. The peak at 465.64  $\text{cm}^{-1}$  might represent the C–C skeleton vibration related to hydrocarbon from phenol and branched alkanes; C–H bending vibration at 1430.35  $\text{cm}^{-1}$  could be attributed to aliphatic hydrocarbon and alkene; the peak at 796.30 was regarded as the C–H bending vibration of aromatic matters with low intensity; the strong C=O stretching vibration correlated phenol and ether could be observed at 1102  $\text{cm}^{-1}$ ; the broad peak at 3318.57  $\text{cm}^{-1}$  demonstrated O–H stretching vibration corresponding to hydroxyl group indicating the water molecules loses intensity in pyrolysis (Liu et al. 2020; Mendez et al. 2013). Compared to the raw biochar, there was the obvious reduction of all the intensities of the peaks at 465.64  $\text{cm}^{-1}$  (C–C skeleton vibration), 796.30  $\text{cm}^{-1}$  (C–H bending vibration), 1102  $\text{cm}^{-1}$  (C=O stretching vibration), and 1430.35  $\text{cm}^{-1}$  (C–H bending vibration) after

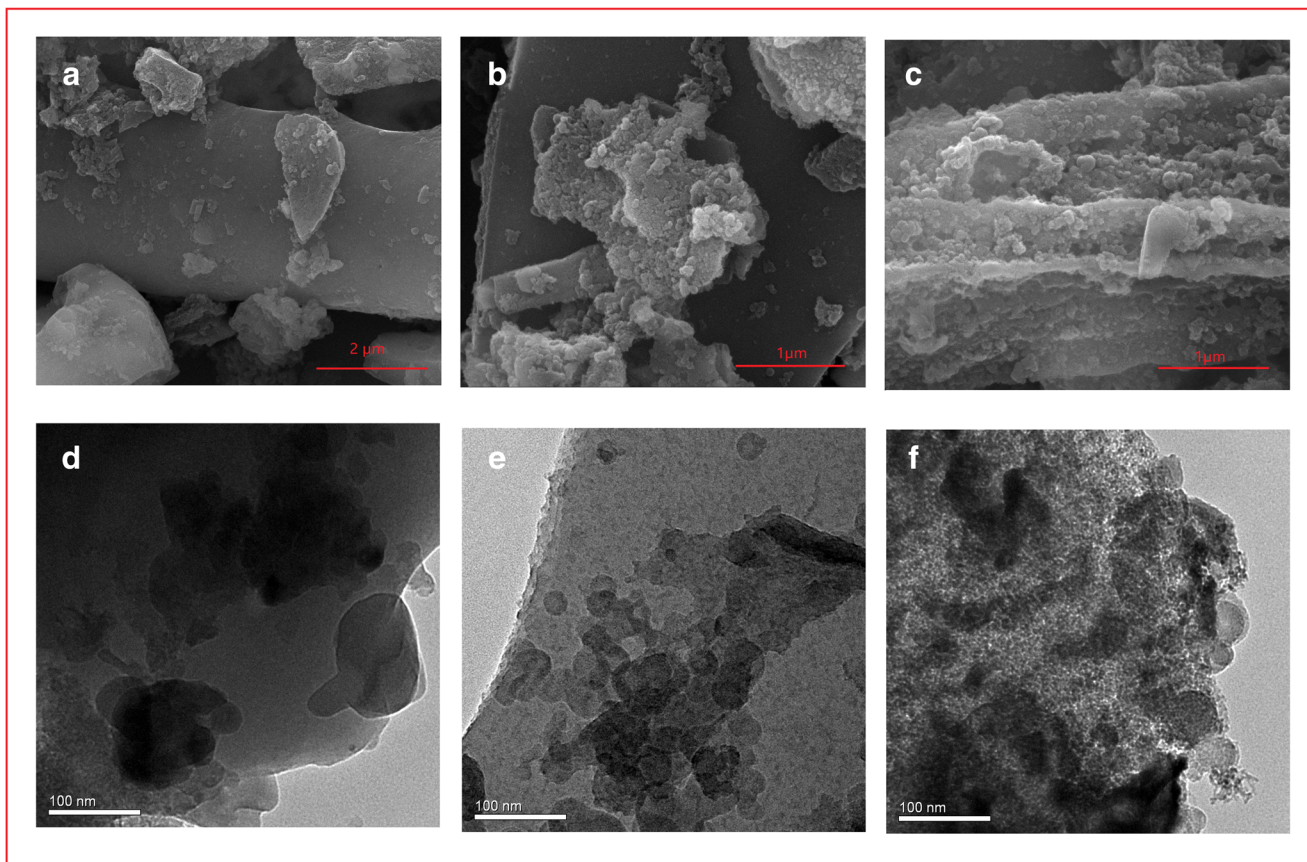


**Fig. 2** Scanning electron microscope (SEM) and transmission electron microscope (TEM) images of biochar before (A, D) and after (B, C, E, F) La (III) and Nd (III) reaction

La(III) and Nd(III) adsorption. This finding revealed the depth engagement of the functional groups such as C–C, C=O, C–H, and -OH in these adsorption reactions.

Figure 3B also exhibited the Raman spectra in the wavelength range of 500–2000  $\text{cm}^{-1}$  on the surface of biochar before and after the Lanthanides sorption. The presence of

the peaks at 1368–1384  $\text{cm}^{-1}$  were and 1588–1600  $\text{cm}^{-1}$  could be assigned to the D and G bands respectively. The peak of the G band was significantly modified after both La(III) and Nd(III) adsorption, which indicated the participation of the  $\text{sp}^2$  carbon through  $\pi$  electrons interaction mechanisms. The changing D band intensity and

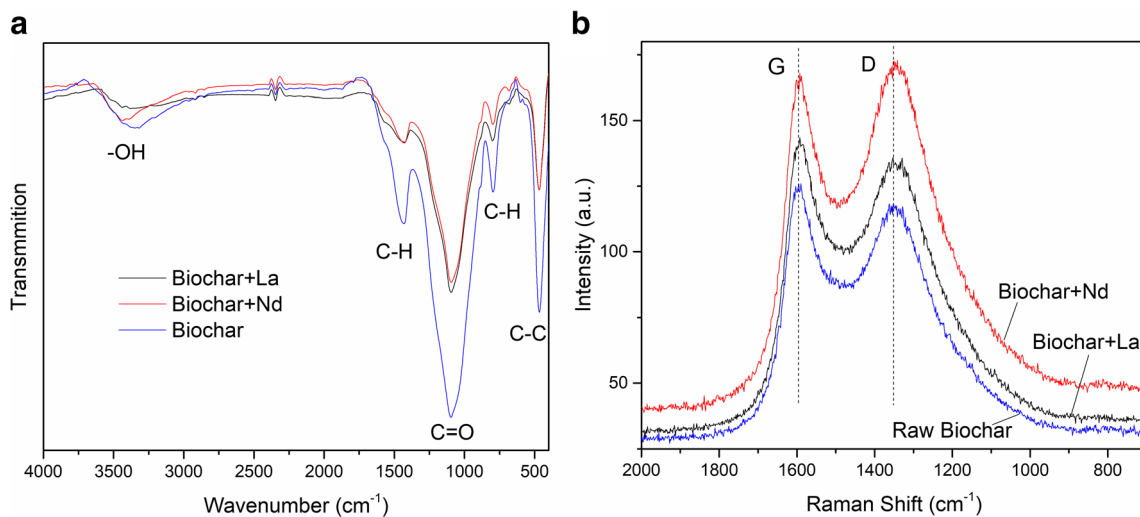


**Fig. 3** FT-IR (A) and Raman (B) spectra of biochar before and after La (III) and Nd (III) reaction

corresponding D/G ratio alteration was ascribed to the disorder of the carbon atom on the biochar surface (Chi et al. 2017; Chia et al. 2012)

### XPS analysis

Figure 4 exhibited the resemble C1s XPS spectra on the surface of biochar before and after La(III) and Nd(III) adsorption. The broadest peaks, which could be assigned to carbon functional groups such as C–C ( $sp^2$ -carbon) and C–C ( $sp^3$ -carbon), all occurred at the location with the binding energy of 284.4 eV and 284.8 eV, (raw biochar: 76.00%, biochar+La:72.70%, biochar+Nd:59.80%). Peaks at 285.4 eV representing C–O groups also could be observed with similar distribution before or after the lanthanides adsorption (raw biochar: 18.06%, biochar+La:18.27%, biochar+Nd:22.29%) (Liu et al. 2020; Lyu et al. 2017). However, the carbonyl groups C–O–C showed a higher percentage of La(III) and Nd(III) adsorbed biochar than the raw material (raw biochar: 5.94%, biochar+La:18.27%, biochar+Nd:22.29%). Referring to the O1s spectra of raw biochar, the peak at 531.5 eV indicated carbonyl bond C=O contained the ketone, lactone, carbonyl, and quinone groups. The presence of carbonyl bond in the carboxylic group such as C–O and O–C=O was also confirmed according to the peaks

at 533.5 eV and 532.6 eV. After La(III) and Nd(III) adsorption, resemble distributions of these oxygen functional groups were observed (Fig. 4).

### Kinetic

To investigate the kinetics of the La(III) and Nd(III) removal, the adsorptions on the biochar were determined as the contact time went by. Figure 5 demonstrated that either the adsorption quantity of the La(III) and Nd(III) adsorption in the aqueous solutions with initial sorbent concentration of 30 mg/L, 50mg/L, and 80mg/L increased in the initial 20 min and rose rapidly until 75 min. Then, they maintained a high level in the contact time range of 75–120 min. All the time nodes exhibited the increasing adsorption quantity with the increasing sorbent dosage. The adsorption percentage of the two rare-earth ions adsorption showed similar growing trends with contact time as the adsorption quantity. Notably, the adsorption percentage of the Nd(III) removal in by biochar dosage of 30 mg/L initially grew more acutely than which using 50 mg/L and 80 mg/L biochar. The straw-derived biochar showed superior capacity in  $La^{3+}$  and  $Nd^{3+}$  adsorption process compared to the previously used material (Table 1).

Two popular kinetics models: pseudo-first-order kinetic model and pseudo-second-order kinetic model, which were most prevalent to illustrate the mechanism of the practical

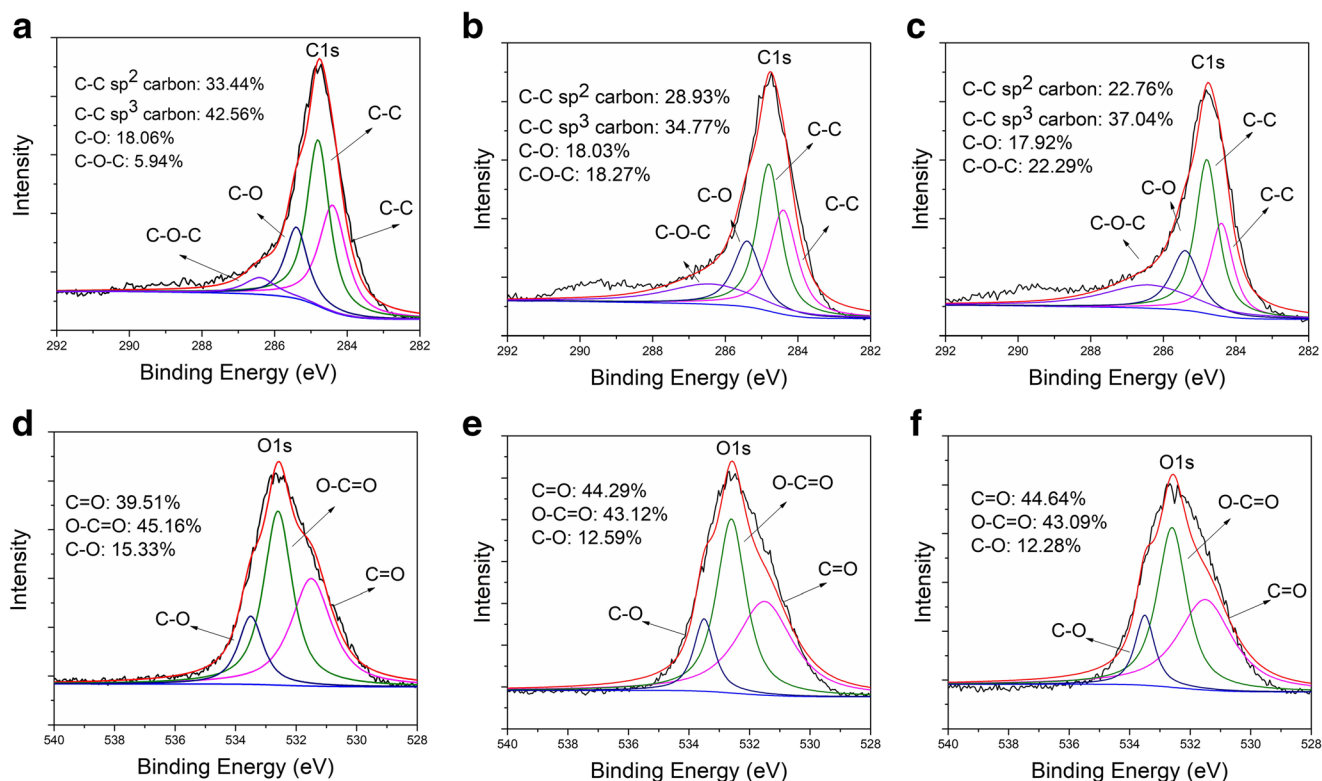


**Fig. 4** High-resolution X-ray photoelectron spectroscopy (XPS) spectra of C1 s before (A) and after La (III) and Nd (III) reaction (B, C) and O1 s before (D) and after La (III) and Nd (III) reaction (E, F)

**Table 1** Adsorption characteristics of La(III) and Nd(III) adsorption on various biochars

Adsorbent	Ion	Adsorption pH	Adsorption Temperature (°C)	$q_{max}$ (mg*g <sup>-1</sup> )	References
Straw derived biochar	La <sup>3+</sup>	5.0	20	80.44	This study
Straw derived biochar	Nd <sup>3+</sup>	5.0	20	71.62	This study
Pectin from durian rind	La <sup>3+</sup>	4.0	25	64.00	(Kusrini et al. 2018)
SiO <sub>2</sub> <sup>+</sup> carboxymethyl chitosan	Nd <sup>3+</sup>	6.9	55	30.23	(Wang et al. 2013)

ion adsorption process on the biochar surface, were employed in this experiment (Tan et al. 2014). The two models were generally expressed in the following form:

$$\ln(q_e - q_t) = \ln q_e - k_1 t \tag{1}$$

$$\frac{t}{q_t} = \frac{1}{k_2 q_e^2} + \frac{t}{q_e} \tag{2}$$

Both the La(III) and Nd(III) removal process fitted the pseudo-second-order kinetic model better than the pseudo-first-order kinetic model based on the kinetic data (Table S1). This result was supported by the previous study about aqueous lanthanides adsorption (Cremel et al. 2007; Kusrini et al. 2018; Tan et al. 2014; Torab-Mostaedi et al. 2013). After the adsorption processes, La and Nd were heterogeneously distributed on the surface of biochar. The chemical sorption and chemisorption on the biochar surface could

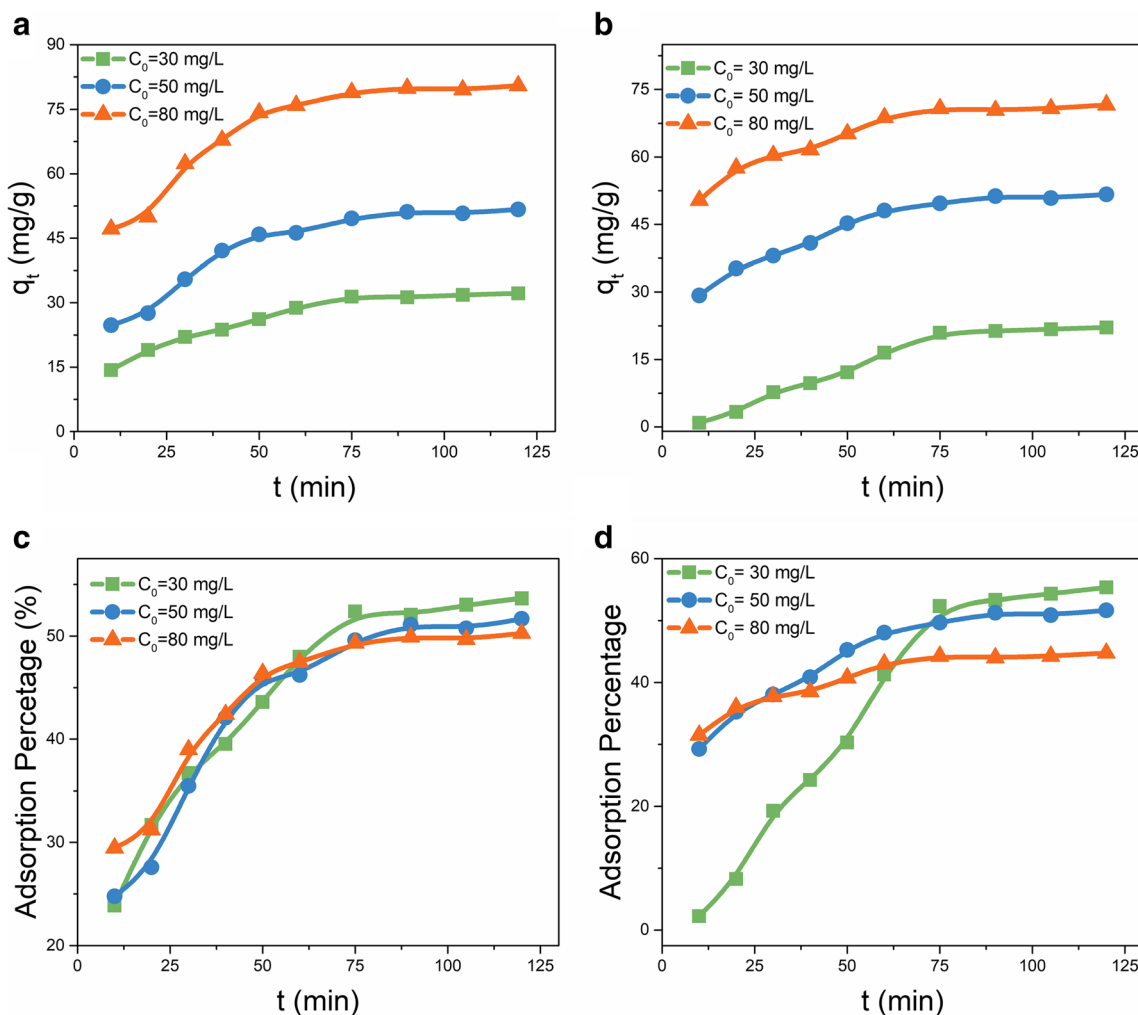


**Fig. 5** Adsorption capacity and percentage of La (III) (A, C) and Nd (III) (B, D) on biochar as a function of contact time

be accountable for this phenomenon. The electrons sharing and exchange occurred between adsorbate and adsorbent accompanying valence forces. The reduction of La and Nd and the complexation between the lanthanides and functional groups could be also found on the biochar surface (Liu and Zhang 2009; Lu et al. 2012; Sheng et al. 2013; Sheng et al. 2014a; Sheng et al. 2014b).

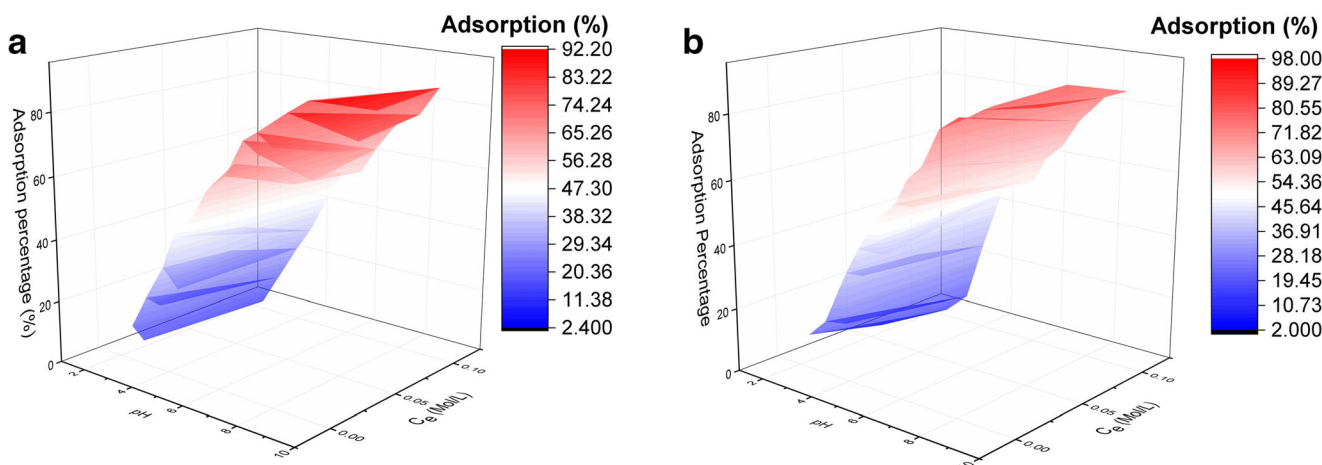
### Effect of pH and ionic strength

Figure 6 depicted that pH was the important factor to influence the adsorption capacity in the La(III) and Nd(III) removal processes. Both the adsorption percentage to the two Lanthanides elements ascended with the increasing pH value. Nevertheless, the growing trends of adsorption capacity were alleviated by the increasing pH. These trends might be mainly ascribed to the functional groups on the biochar surface such as carboxylate and hydroxyl (Abdel-Fattah et al. 2015). At a low pH level, these functional groups were presented in the positive charges form on the biochar surface since they were protonated in the proton-rich acidic solution. Thus, the electrostatic effects made the lanthanides cations repulsed by the positively charged biochar surface. In addition, the contaminant cations had to compete for the available binding site on the sorbent surface with the aqueous cations like  $H^+$  and  $H_3O^+$  (Abdel-Fattah et al. 2015; Oh et al. 2012). As the pH value increased, copious binding sites were released for the adsorbate and the functional groups were deprotonated so that the competition between the Lanthanides cations the aqueous protons was moderated (Lu et al. 2012). the biochar surface changed into a negatively charged form when  $pH > pH_{pzc}$ , so its capture capacity of the pollutant cations was further strengthened. Meanwhile, since the reserved available adsorption site for releasing reduced constantly, the increasing trends of the adsorption capacity were alleviated with the inducing pH value (Tan et al. 2015).

In contrast, the adsorption capacities for the La(III) and Nd(III) removal were slightly changed and robust with the ionic strength (Fig. 6). The Nd(III) removal process did not strongly depend on the interfering ion. However, the adsorption percentage La(III) slightly decreased with the presence of the interfering ion  $Na^+$ . Previous researches also reported similar results about the Lanthanides adsorption. This decrease was caused by the presence of  $Na^+$  might be accountable for this finding because it resulted in the reduction of the electrostatic interaction on the biochar surface (Kusrini et al. 2018).

### Adsorption isotherm and thermodynamic

The isotherms of La(III) and Nd(III) adsorption at the temperature of 293K, 313K, and 333K were exhibited in Fig. 7. Either adsorption capacity of the two lanthanides removal process ascended with the growing temperature. This phenomenon indicated the high-temperature favor of the La(III) and Nd(III) uptake on the biochar surface. To investigate the mechanism and quantization of the adsorption processes, two empirical models extensively used for the simulation of adsorption on biochar: Langmuir, Freundlich, and Sips model, were employed to fit the experimental data of these aqueous contaminant removals (Tan et al. 2015). Langmuir model is a linear equation described as:  $\frac{1}{q_e} = \frac{1}{q_{max}} + \frac{1}{bq_{max}} \frac{1}{C_e} \cdot q_{max}$  (mg/g) indicates the maximum loading quantity of adsorptive lanthanides by the unit weight of biochar;  $q_e$  (mg/g) represents the adsorbates amount of unit weight of sorbent at equilibrium concentration;  $b$  (L/mg) is the Langmuir constants depending on adsorptive energy;  $C_e$  represents the equilibrium concentration of La(III) and Nd(III) anions (mg/g) (Inyang et al. 2015). Freundlich model could be expressed as  $q_e = K_F C_e^n$  or the modified linear form:  $\log q_e = \log K_F + n \log C_e$ .  $K_F$  (( $mg^{1-n} \cdot L^n$ )/g) represents the Freundlich constant interrelated to the adsorption capacity;  $n$  indicates the dependent degree in



**Fig. 6** Effect of pH and foreign ions on La (III) (A) and Nd (III) (B) adsorption to biochar

**Table 2** Constants of Freundlich and Langmuir isotherm of La(III) and Nd(III) adsorption on biochar

Absorbate	T (K)	Freundlich			Langmuir			Sips			
		$K_f$ (mg <sup>1-n</sup> ·L <sup>n</sup> /g)	$n$	$R^2$	$q_{max}$ (mg/g)	$b$ (L/mg)	$R^2$	$q_{max}$ (mg/g)	$K$ (mg <sup>1-n</sup> ·L <sup>n</sup> /g)	$n$	$R^2$
La (II)	293	2.4099	0.9480	0.9143	585.76	0.0039	0.9207	107.65	0.0011	2.1608	0.9517
	313	5.5888	0.7805	0.9187	291.77	0.0129	0.9410	121.16	0.0024	2.0486	0.9768
	333	10.6253	0.6532	0.9747	242.51	0.0238	0.9895	199.60	0.0214	1.1435	0.9877
Nd (II)	293	7.6607	0.5950	0.9755	137.55	0.0259	0.9886	123.99	0.0237	1.0856	0.9852
	313	14.3975	14.3975	0.9818	127.86	0.0475	0.9736	295.72	0.0411	0.6112	0.9774
	333	32.5613	0.3213	0.9618	129.77	0.1130	0.9186	2944.49	0.0111	0.3309	0.9488

adsorptive Lanthanides removal process at the equilibrium concentration (Kusrini et al. 2018). Sips model could be expressed as  $q_e = q_{max} \frac{KC_e^n}{1+KC_e^n}$ .  $q_{max}$  (mg/g) represents the theoretical maximum adsorptive capacity for lanthanides by unit weight;  $q_e$  (mg/g) indicates the adsorbates amount of unit weight of biochar at equilibrium concentration;  $K$  ((mg<sup>1-n</sup>·L<sup>n</sup>/g) represents the Sips constant interrelated to the adsorption capacity;  $C_e$  represents the equilibrium concentration of lanthanides anions (mg/g) (Lima et al. 2019; Liu and Liu 2008). Both the La(III) and Nd(III) adsorptive processes were observed to fit either Langmuir or Freundlich model (Table 2). Langmuir model could be effectually applied to the sorbent with a monolayer surface. Freundlich model is more apposite for the adsorption on the multi-layer surface rather than a restricted monolayer

(Chang et al. 2017; Hu et al. 2017a; Hu et al. 2017b; Hu et al. 2016; Hu et al. 2011; Inyang et al. 2015; Kim et al. 2013). Sips model was always employed when the experiment results were represented by the isotherm form of Langmuir or Freundlich model was uncertain. In this regard, the practical adsorbent was biochar, which might combine homogeneous and heterogenous partial surface resulted from different pyrolysis temperature and retention time (Oh et al. 2012; Tan et al. 2015). This randomness of the internal surface led to the great fitting of the La(III) and Nd(III) adsorption data to both Langmuir and Freundlich models. The goodness of fitting for the Sips model further proved this combination of adsorption modes.

Several vital thermodynamic parameters such as standard entropy ( $\Delta S_0$ ), standard enthalpy ( $\Delta H_0$ ), and standard Gibbs

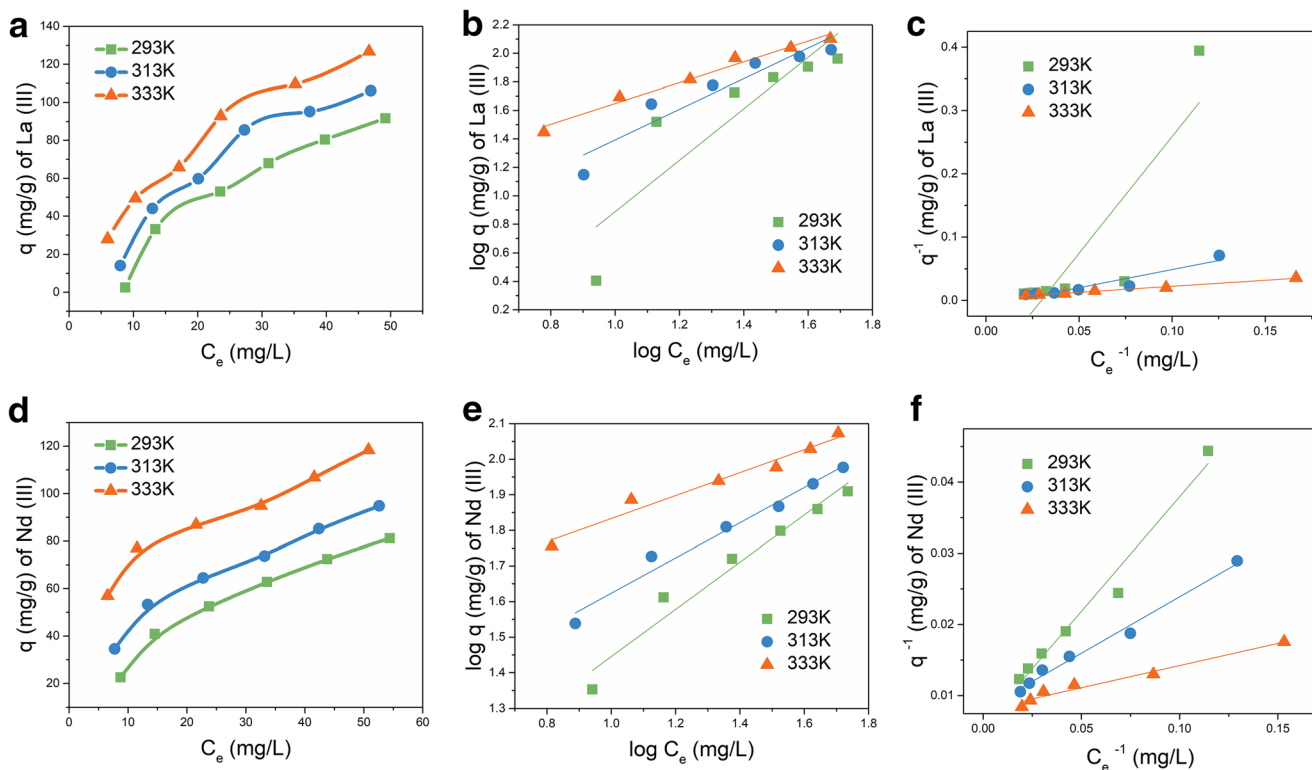


**Fig. 7** Isotherm and Fitting results of Langmuir and Freundlich adsorption isotherms of La (III) (A, C, E) and Nd (III) (B, D, F) adsorption on biocha



**Table 3** Values of thermodynamic parameters for the adsorption of La(III) and Nd(III) on biochar

Adsorbate	$\Delta H^0$ (kJ/Mol)	$\Delta S^0$ (J*Mol <sup>-1</sup> *K <sup>-1</sup> )	$\Delta G^0$ (KJ/mol)		
			293K	313K	333K
La (II)	35.39	104.71	-40.04	-42.77	-45.51
Nd (II)	16.71	119.41	-34.97	-37.36	-39.75

free energy ( $\Delta G_0$ ) were employed to evaluate the thermodynamic of the process (Table 3). The parameters were taken into calculation following the coming equations:

$$K_d = \frac{C_0 - C_e}{C_e} \frac{V}{m}, \quad (3)$$

$$\ln K_d = \frac{\Delta S^0}{R} - \frac{\Delta H^0}{RT}, \quad (4)$$

$$\Delta G^0 = \Delta H^0 - T\Delta S^0. \quad (5)$$

$C_0$  (mg/L) indicates the initial concentration and  $C_e$  (mg/L) is the equilibration concentration of the Lanthanides contaminant in aqueous solution respectively;  $V$  (mL) and  $m$  (g) represent the volume and mass of biochar as the sorbent;  $T$  (K) and  $R$  (8.314 J·mol<sup>-1</sup>·K<sup>-1</sup>) are related temperatures in Kelvin and the ideal gas constant. Table 3 depicted the positive values of standard enthalpy ( $\Delta H_0$ ) in La(III) and Nd(III) adsorption processes, which indicated the endothermicity of these reactions. The processes also could be asserted as spontaneous reactions according to their positive and negative values of standard entropy ( $\Delta S_0$ ) and standard Gibbs free energy ( $\Delta G_0$ ) respectively. Moreover, the absolute value of standard Gibbs free energy ( $\Delta G_0$ ) increased with the increasing temperature. This result demonstrated the temperature favor of the spontaneity in these La(III) and Nd(III) removal processes and coincided with the isotherm results referred to above. This nature proved the potential of biochar as the low-cost sorbent for continuous lanthanides removal. These thermodynamic parameters also indicate lanthanide adsorptions are both physical and chemical adsorptions. Generally, physical adsorption takes advantage of van der Waals force while chemical adsorption takes chemical bond as the adsorptive attraction. The Gibbs free energy of physical adsorption usually falls in the interval of -20 to 0 and kJ/mol and the  $\Delta G^0$  of chemical adsorption was in the range of -400 to -80 kJ/mol (Liu and Zhang 2009). In this study, the Gibbs free energy of La(III) and Nd(III) adsorption were both in the interval of -50 to -35 kJ/mol. This finding implied the La(III) and Nd(III) adsorption using biochar was the combination of physical and chemical adsorptions. This assumption was further proved by the low values of  $\Delta H_0$  in both lanthanide adsorption.

Previous studies about the adsorption on biochar found similar spontaneity, endothermic nature, and temperature favor because the enhanced temperature and heat could offer external energy for the lanthanides ions binding onto the electropolymerized biochar surface in aqueous solution (Liu and Zhang 2009; Parshetti et al. 2014; Sun et al. 2014).

## Conclusion

This study has clarified the process and mechanism of aqueous La(III) and Nd(III) removal by straw-derived biochar through the systematic survey. The kinetic result showed a great fit to the pseudo-second-order model. The findings from experiment data also depicted that the adsorption capacity was strongly positively correlated to pH value while only slightly altered and robust in La(III) and Nd(III) adsorption. Referring to the isotherm, the Sips model could supply significant simulation for the sorption. Endothermic nature, spontaneity, and temperature favor of the adsorption reaction could be observed from thermodynamic parameters. Either La(III) or Nd(III) adsorption was the combination of physical and chemical adsorption. This work provides ample evidence to assert biochar as an efficient adsorbent for the removal of La(III) and Nd(III) in aqueous solutions.

**Supplementary Information** The online version contains supplementary material available at <https://doi.org/10.1007/s11356-021-13988-2>.

**Author contribution** QZ conceived, designed, and performed the experiments, analyzed data, and wrote the manuscript. YW, ZX, and ZY revised the manuscript. All authors read and approved the final manuscript.

**Data availability** Not applicable

## Declarations

**Ethics approval** Not applicable

**Consent to participate** All participants provided informed verbal consent.

**Consent for publication** All authors agreed to publish on this journal.

**Competing interests** The authors declare no competing interests.

## References

- Abdel-Fattah TM, Mahmoud ME, Ahmed SB, Huff MD, Lee JW, Kumar S (2015) Biochar from woody biomass for removing metal contaminants and carbon sequestration. *J Ind Eng Chem* 22:103–109
- Ahmad M, Lee SS, Dou X, Mohan D, Sung JK, Yang JE, Ok YS (2012) Effects of pyrolysis temperature on soybean stover- and peanut shell-derived biochar properties and TCE adsorption in water. *Bioresour Technol* 118:536–544
- Ahmad M, Rajapaksha AU, Lim JE, Zhang M, Bolan N, Mohan D, Vithanage M, Lee SS, Ok YS (2014) Biochar as a sorbent for contaminant management in soil and water: a review. *Chemosphere* 99:19–33
- Antón-Herrero R, García-Delgado C, Alonso-Izquierdo M, García-Rodríguez G, Cuevas J, Eymar E (2018) Comparative adsorption of tetracyclines on biochars and stevensite: Looking for the most effective adsorbent. *Appl Clay Sci* 160:162–172
- Cao X, Harris W (2010) Properties of dairy-manure-derived biochar pertinent to its potential use in remediation. *Bioresour Technol* 101:5222–5228
- Cao X, Ma L, Liang Y, Gao B, Harris W (2011) Simultaneous immobilization of lead and atrazine in contaminated soils using dairy-manure biochar. *Environ Sci Technol* 45:4884–4889
- Chang K, Sun Y, Ye F, Li X, Sheng G, Zhao D, Linghu W, Li H, Liu J (2017) Macroscopic and molecular study of the sorption and co-sorption of graphene oxide and Eu(III) onto layered double hydroxides. *Chem Eng J* 325:665–671
- Chen W, Meng J, Han X, Lan Y, Zhang W (2019) Past, present, and future of biochar. *Biochar* 1:75–87
- Chi T, Zuo J, Liu F (2017) Performance and mechanism for cadmium and lead adsorption from water and soil by corn straw biochar. *Front Environ Sci Eng* 11:15
- Chia CH, Gong B, Joseph SD, Marjo CE, Munroe P, Rich AM (2012) Imaging of mineral-enriched biochar by FTIR, Raman and SEM-EDX. *Vibrat Spect* 62:248–257
- Cremel S, Zamama O, Dossot M, Lambert J, Humbert B, Ehrhardt J-J (2007) Sorption of Eu<sup>3+</sup> on dickite particles studied by Raman, luminescence, and X-ray photoelectron spectroscopies. *Comptes Rendus Chimie* 10:1050–1059
- Dong X, Ma LQ, Li Y (2011) Characteristics and mechanisms of hexavalent chromium removal by biochar from sugar beet tailing. *J Hazard Mater* 190:909–915
- Galunin E, Alba MD, Santos MJ, Abrão T, Vidal M (2010) Lanthanide sorption on smectitic clays in presence of cement leachates. *Geochim Cosmochim Acta* 74:862–875
- Hu XJ, Wang JS, Liu YG, Li X, Zeng GM, Bao ZL, Zeng XX, Chen AW, Long F (2011) Adsorption of chromium (VI) by ethylenediamine-modified cross-linked magnetic chitosan resin: isotherms, kinetics and thermodynamics. *J Hazard Mater* 185:306–314
- Hu B, Ye F, Ren X, Zhao D, Sheng G, Li H, Ma J, Wang X, Huang Y (2016) X-ray absorption fine structure study of enhanced sequestration of U(VI) and Se(IV) by montmorillonite decorated with zero-valent iron nanoparticles. *Environ Sci: Nano* 3:1460–1472
- Hu B, Chen G, Jin C, Hu J, Huang C, Sheng J, Sheng G, Ma J, Huang Y (2017a) Macroscopic and spectroscopic studies of the enhanced scavenging of Cr(VI) and Se(VI) from water by titanate nanotube anchored nanoscale zero-valent iron. *J Hazard Mater* 336:214–221
- Hu B, Huang C, Li X, Sheng G, Li H, Ren X, Ma J, Wang J, Huang Y (2017b) Macroscopic and spectroscopic insights into the mutual interaction of graphene oxide, Cu(II), and Mg/Al layered double hydroxides. *Chem Eng J* 313:527–534
- Inyang MI, Gao B, Yao Y, Xue Y, Zimmerman A, Mosa A, Pullammanappallil P, Ok YS, Cao X (2015) A review of biochar as a low-cost adsorbent for aqueous heavy metal removal. *Crit Rev Environ Sci Technol* 46:406–433
- Johnson BE, Santschi PH, Chuang CY, Otsuka S, Addleman RS, Douglas M, Rutledge RD, Chouyyok W, Davidson JD, Fryxell GE, Schwantes JM (2012) Collection of lanthanides and actinides from natural waters with conventional and nanoporous sorbents. *Environ Sci Technol* 46:11251–11258
- Kappler A, Fischer D, Oberbeckmann S, Schernewski G, Labrenz M, Eichhorn KJ, Voit B (2016) Analysis of environmental microplastics by vibrational microspectroscopy: FTIR, Raman or both? *Anal Bioanal Chem* 408:8377–8391
- Kim WK, Shim T, Kim YS, Hyun S, Ryu C, Park YK, Jung J (2013) Characterization of cadmium removal from aqueous solution by biochar produced from a giant Miscanthus at different pyrolytic temperatures. *Bioresour Technol* 138:266–270
- Kumar S, Kar AS, Tomar BS, Bhattacharyya D (2012) X-ray absorption fine structure spectroscopy study of Eu(III) sorption products onto amorphous silica and  $\gamma$ -alumina: Effect of pH and substrate. *Polyhedron* 33:33–40
- Kusrini E, Wicaksono W, Gunawan C, Daud NZA, Usman A (2018) Kinetics, mechanism, and thermodynamics of lanthanum adsorption on pectin extracted from durian rind. *J Environ Chem Eng* 6:6580–6588
- Kuta J, Wander MCF, Wang Z, Jiang S, Wall NA, Clark AE (2011) Trends in Ln(III) Sorption to Quartz Assessed by Molecular Dynamics Simulations and Laser-Induced Fluorescence Studies. *J Phys Chem C* 115:21120–21127
- Lehmann J, Bossio DA, Kogel-Knabner I, Rillig MC (2020) The concept and future prospects of soil health. *Nat Rev Earth Environ* 1:544–553
- Liao Q, Zou D, Pan W, Linghu W, Shen R, Li X, Asiri AM, Alamry KA, Sheng G, Zhan L, Wu X (2018) Highly efficient capture of Eu(III), La(III), Nd(III), Th(IV) from aqueous solutions using g-C<sub>3</sub>N<sub>4</sub> nanosheets. *J Mol Liq* 252:351–361
- Lima EC, Hosseini-Bandegharai A, Moreno-Piraján JC, Anastopoulos I (2019) A critical review of the estimation of the thermodynamic parameters on adsorption equilibria. Wrong use of equilibrium constant in the Van't Hoff equation for calculation of thermodynamic parameters of adsorption. *J Mol Liq* 273:425–434
- Liu Y, Liu Y-J (2008) Biosorption isotherms, kinetics and thermodynamics. *Sep Purif Technol* 61:229–242
- Liu Z, Zhang FS (2009) Removal of lead from water using biochars prepared from hydrothermal liquefaction of biomass. *J Hazard Mater* 167:933–939
- Liu N, Zhang Y, Xu C, Liu P, Lv J, Liu Y, Wang Q (2020) Removal mechanisms of aqueous Cr(VI) using apple wood biochar: a spectroscopic study. *J Hazard Mater* 384:121371
- Lu H, Zhang W, Yang Y, Huang X, Wang S, Qiu R (2012) Relative distribution of Pb<sup>2+</sup> sorption mechanisms by sludge-derived biochar. *Water Res* 46:854–862
- Lyu H, Tang J, Huang Y, Gai L, Zeng EY, Liber K, Gong Y (2017) Removal of hexavalent chromium from aqueous solutions by a novel biochar supported nanoscale iron sulfide composite. *Chem Eng J* 322:516–524
- Mendez A, Tarquis AM, Saa-Requejo A, Guerrero F, Gasco G (2013) Influence of pyrolysis temperature on composted sewage sludge biochar priming effect in a loamy soil. *Chemosphere* 93:668–676
- Meunier N, Drogui P, Montane C, Hausler R, Mercier G, Blais JF (2006) Comparison between electrocoagulation and chemical precipitation for metals removal from acidic soil leachate. *J Hazard Mater* 137:581–590
- Mohan D, Sarswat A, Ok YS, Pittman CU Jr (2014) Organic and inorganic contaminants removal from water with biochar, a renewable, low cost and sustainable adsorbent—a critical review. *Bioresour Technol* 160:191–202
- Oehmen A, Viegas R, Velizarov S, Reis MAM, Crespo JG (2006) Removal of heavy metals from drinking water supplies through the ion exchange membrane bioreactor. *Desalination* 199:405–407

- Oh T-K, Choi B, Shinogi Y, Chikushi J (2012) Effect of pH Conditions on Actual and Apparent Fluoride Adsorption by Biochar in Aqueous Phase. *Water Air Soil Pollut* 223:3729–3738
- Parks JM, Johs A, Podar M, Bridou R, Hurt RA, Smith SD, Tomanicek SJ, Qian Y, Brown SD, Brandt CC, Palumbo AV, Smith JC, Wall JD, Elias DA, Liang LY (2013) The Genetic Basis for Bacterial Mercury Methylation. *Science* 339:1332–1335
- Parshetti GK, Chowdhury S, Balasubramanian R (2014) Hydrothermal conversion of urban food waste to chars for removal of textile dyes from contaminated waters. *Bioresour Technol* 161:310–319
- Sharma P, Tomar R (2011) Sorption behaviour of nanocrystalline MOR type zeolite for Th(IV) and Eu(III) removal from aqueous waste by batch treatment. *J Colloid Interface Sci* 362:144–156
- Sheng G, Dong H, Shen R, Li Y (2013) Microscopic insights into the temperature-dependent adsorption of Eu(III) onto titanate nanotubes studied by FTIR, XPS, XAFS and batch technique. *Chem Eng J* 217:486–494
- Sheng G, Yang Q, Peng F, Li H, Gao X, Huang Y (2014a) Determination of colloidal pyrolusite, Eu(III) and humic substance interaction: A combined batch and EXAFS approach. *Chem Eng J* 245:10–16
- Sheng GD, Yang ST, Li YM, Gao X, Huang YY, Hu J, Wang XK (2014b): Retention mechanisms and microstructure of Eu(III) on manganese dioxide studied by batch and high resolution EXAFS technique. *Radiochim Acta* 102
- Shi W-Q, Zhao Y-L, Chai Z-F (2012) Nuclear and radiochemistry in China: present status and future perspectives. *Radiochim Acta* 100:529–539
- Sun J, Lian F, Liu Z, Zhu L, Song Z (2014) Biochars derived from various crop straws: characterization and Cd(II) removal potential. *Ecotoxicol Environ Saf* 106:226–231
- Tan X, Ren X, Chen C, Wang X (2014) Analytical approaches to the speciation of lanthanides at solid-water interfaces. *TrAC Trend Anal Chem* 61:107–132
- Tan X, Liu Y, Zeng G, Wang X, Hu X, Gu Y, Yang Z (2015) Application of biochar for the removal of pollutants from aqueous solutions. *Chemosphere* 125:70–85
- Torab-Mostaedi M, Asadollahzadeh M, Hemmati A, Khosravi A (2013) Biosorption of lanthanum and cerium from aqueous solutions by grapefruit peel: equilibrium, kinetic and thermodynamic studies. *Res Chem Intermed* 41:559–573
- Wang F, Zhao J, Zhou H, Li W, Sui N, Liu H (2013) O-carboxymethyl chitosan entrapped by silica: preparation and adsorption behaviour toward neodymium (III) ions. *J Chem Technol Biotechnol* 88:317–325
- Wang S, Gao B, Zimmerman AR, Li Y, Ma L, Harris WG, Migliaccio KW (2015) Removal of arsenic by magnetic biochar prepared from pinewood and natural hematite. *Bioresour Technol* 175:391–395
- Zhou Q, Liao B, Lin L, Qiu W, Song Z (2018) Adsorption of Cu(II) and Cd(II) from aqueous solutions by ferromanganese binary oxide-biochar composites. *Sci Total Environ* 615:115–122

**Publisher's note** Springer Nature remains neutral with regard to jurisdictional claims in published maps and institutional affiliations.